



Queensland University of Technology
Brisbane Australia

This is the author's version of a work that was submitted/accepted for publication in the following source:

Frost, Ray L. & Palmer, Sara J. (2009) The effect of synthesis temperature on the formation of hydrotalcites in Bayer liquor : a vibrational spectroscopic analysis. *Applied Spectroscopy*, 63(7), pp. 748-752.

This file was downloaded from: <http://eprints.qut.edu.au/41980/>

© Copyright 2009 Society for Applied Spectroscopy

Notice: *Changes introduced as a result of publishing processes such as copy-editing and formatting may not be reflected in this document. For a definitive version of this work, please refer to the published source:*

<http://dx.doi.org/10.1366/000370209788701152>

1 **The effect of synthesis temperature on the formation of hydrotalcites**
2 **in Bayer liquor—a vibrational spectroscopic analysis**

3

4 **Sara J. Palmer and Ray L. Frost***

5 *Inorganic Materials Research Program, School of Physical and Chemical Sciences, Queensland*

6 *University of Technology, Queensland, Australia.*

7 *Fax: +61 7 3138 1804; Tel +61 7 3138 2407; E-mail: r.frost@qut.edu.au*

8

9 **ABSTRACT**

10 The seawater neutralisation process is currently used in the Alumina industry to
11 reduce the pH and dissolved metal concentrations in bauxite refinery residues,
12 through the precipitation of Mg, Al, and Ca hydroxide and carbonate minerals. This
13 neutralisation method is very similar to the co-precipitation method used to synthesise
14 hydrotalcite ($\text{Mg}_6\text{Al}_2(\text{OH})_{16}\text{CO}_3 \cdot 4\text{H}_2\text{O}$). This study looks at the effect of temperature
15 on the type of precipitates that form from the seawater neutralisation process of Bayer
16 liquor. The Bayer precipitates have been characterised by a variety of techniques,
17 including X-ray diffraction, Raman spectroscopy and infrared spectroscopy. The
18 mineralogical composition of Bayer precipitates largely includes hydrotalcite,
19 hydromagnesite, and calcium carbonate species. XRD determined that Bayer
20 hydrotalcites that are synthesised at 55 °C have a larger interlayer distance, indicating
21 more anions are removed from Bayer liquor. Vibrational spectroscopic techniques
22 have identified an increase in hydrogen bond strength for precipitates formed at 55
23 °C, suggesting the formation of a more stable Bayer hydrotalcite. Raman
24 spectroscopy identified the intercalation of sulfate and carbonate anions into Bayer
25 hydrotalcites using these synthesis conditions.

26

27 **KEYWORDS:** hydrotalcite, Bayer liquor, characterisation, spectroscopy

28

29 INTRODUCTION

30

31 The Bayer process produces large quantities of the highly alkaline bauxite refinery
32 residue (red mud), which consist of a variety of hazardous anions. Red mud
33 requires treatment before it can be safely discharged into the environment or
34 stored. The seawater neutralisation of red mud reduces both the pH and dissolved
35 metal concentrations of the residue, and has been employed in a number of
36 refineries around the world. This is achieved through the precipitation of Mg, Ca,
37 and Al hydroxide and carbonate minerals [1]. The formation of these compounds
38 removes oxy-anions of transition metals through a combination of intercalation
39 and adsorption mechanisms.

40

41 Hydrotalcites consist of stacked layers of metal cations (M^{2+} and M^{3+}) similar to
42 brucite-like structures. Substitution of divalent cations for trivalent ones, of similar
43 radii, gives rise to positively charged layers [2, 3]. The general formula for these
44 structures is: $[M^{2+}_{1-x} M^{3+}_x(OH)_2]^{x+} A^{m-}_{x/m} \cdot nH_2O$, where M^{2+} is a divalent cation,
45 M^{3+} is a trivalent cation, and A an interlamellar anion with charge m-. Hydrotalcite
46 phases exist for $0.2 \leq x \leq 0.33$ [4]. The resultant positive charge, caused by the
47 substitution of Al, is neutralised through the intercalation and adsorption of
48 anions. The affinity of anions for the interlayer region is based on charge density
49 and size. Carbonate has a high affinity for the hydrotalcite interlayer, which limits
50 the removal of other anions from solution if present in high concentrations.

51

52 Hydrotalcites have been synthesised using Bayer refinery liquors under seawater
53 neutralisation (SWN) conditions. This investigation will enable the identification
54 of the type of minerals that form during the SWN of bauxite refinery residues, and
55 the mechanism of formation. This study is looking at determining the most stable
56 precipitate that forms at different temperatures. It is proposed that different
57 precipitates will form depending on the temperature of the resultant solution
58 during the SWN process. Therefore, any structural changes that result from
59 increasing temperatures need to be assessed to see if there is any effect on the
60 formation of Bayer hydrotalcite. The mechanism for the intercalation of different
61 anions and the characterisation of the products of the seawater neutralisation of red
62 mud have previous been investigated by the authors [5, 6].

63

64 **EXPERIMENTAL**

65

66 Supernatant liquor (SNL) from an Australian alumina refinery was neutralised
67 with seawater (SW), collected from Inskip Point, QLD, Australia in October 2008.
68 The chemical composition of SNL and seawater can be found in Table 1. The
69 average initial pH value for SNL is 12.40, and a final pH value of around 9 was
70 obtained once the SNL had been neutralised with seawater. Dependent on the
71 desired synthesis temperature, the Bayer liquor was cooled using an ice water bath
72 and heated on a hotplate to 0, 25, 55, and 75 °C before the addition of 4.5 times
73 the volume of seawater to Bayer liquor. Seawater was added to the liquor at a rate
74 of 5 mL a minute. The mixture was continuously stirred for 2 hours before being
75 vacuum filtered and washed thoroughly with de-ionised water. The precipitate was
76 dried in an oven (85°C) overnight, to remove any surface water.

77

78 Characterisation of the precipitates included XRD, Raman spectroscopy, and
79 infrared spectroscopy. X-Ray diffraction patterns were collected using a Philips
80 X'pert wide angle X-Ray diffractometer, operating in step scan mode, with Cu K α
81 radiation (1.54052 Å). The Fourier Transform Raman spectroscopy (FT-Raman)
82 analyses were performed on powder samples using a Perkin Elmer System 2000
83 Fourier transform spectrometer equipped with a Raman accessory comprising a
84 Spectron Laser Systems SL301 Nd:YAG laser operating at a wavelength of 1064
85 nm. Infrared spectra were obtained using a Nicolet Nexus 870 FTIR spectrometer
86 with a smart endurance single bounce diamond ATR cell. Spectra over the 4000-
87 525 cm⁻¹ range were obtained by the co-addition of 128 scans with a resolution of
88 4 cm⁻¹ and a mirror velocity of 0.6329 m/s.

89

90 Spectral manipulation such as baseline correction, smoothing, and normalisation
91 was performed using the GRAMS® software package (Galactic Industries
92 Corporation, Salem, NH, USA). For more information on the experimental and
93 analysis techniques used, refer to previous work by the authors [6, 7].

94

95

96 **RESULTS AND DISCUSSION**

97

98 **X-Ray Diffraction**

99

100 The X-ray diffraction patterns of the precipitates and the corresponding reference
101 patterns are given in Figure 1. The results show that multiple phases precipitate
102 during the SWN process, in particular hydrotalcite-like structures, and calcium and
103 magnesium carbonate species. The main peak at around $11^\circ 2\theta$ (d_{003} plane peak),
104 is assigned to hydrotalcite (00-035-0965). The broadness of the hydrotalcite peaks
105 indicates that poorly crystalline Bayer hydrotalcites are formed under these
106 synthesis conditions. For more crystalline products, a slower addition rate is
107 required along with a longer synthesis period. However, these studies are based on
108 real scenarios in the Alumina industry. The crystallinity of these Bayer
109 hydrotalcites decrease with increasing temperature, shown by the broadening of
110 the 2 peaks at $60^\circ 2\theta$. The d_{003} spacing of the synthesised Bayer hydrotalcites
111 (BHT) from 0°C to 75°C are 7.71, 7.82, 7.93, and 7.79 Å, respectively. The d_{003}
112 plane peak represents the interlayer distance between the hydroxyl layers of the
113 hydrotalcite structure. The basal spacing for the Bayer hydrotalcites increased with
114 increasing temperature, suggesting that the removal ability of hydrotalcites formed
115 from the co-precipitation method increase up to 55°C . Based on the results of this
116 study, the synthesis of Bayer hydrotalcites formed at 55°C appears to be the most
117 effective in the removal of anions from Bayer liquors. Bayer hydrotalcites that
118 formed at 75°C , showed a reduction in interlayer distance. This reduction is
119 believed to be due to the dehydration of the interlayer region of the hydrotalcite
120 structure at these increased temperatures. Therefore, for optimal removal of anions
121 from Bayer liquors, it is suggested that temperatures between 25 and 55°C should
122 be used in the seawater neutralisation process.

123

124 The elemental composition (Energy dispersive X-ray spectroscopy - EDX) of the
125 Bayer hydrotalcites indicates that the SWN process produces hydrotalcites with a
126 Mg:Al ratio between 3 and 4, with the average value of 3.5, for the hydrotalcites
127 prepared at 0 , 25 , and 55°C . The Mg:Al ratios are 3.4, 3.8, and 3.4, respectively.
128 The precipitate formed at 75°C resulted in a Mg:Al ratio of 6.8. This large

129 increase in Mg:Al ratio is due to the precipitation of hydromagnesite, however, it
130 is thought a Mg:Al ratio of around 3.5 is still obtained at 75 °C, due to minimal
131 changes observed in other techniques used. The elements detected using EDX are
132 Mg, Al, Ca, S, O, C, and Cl. No significant changes were observed in S
133 concentrations, therefore, the synthesis temperature does not appear to have an
134 effect on the uptake of sulfate anions. Apart from carbonate, sulfate, and
135 hydroxide, no other anions are thought to be adsorbed or intercalated into these
136 structures.

137

138 Another predominant phase that formed during the SWN process is aragonite
139 (CaCO_3 – orthorhombic crystal structure). This mineral phase appears to be more
140 crystalline than hydrotalcite, and appears to form predominantly at 25 and 55 °C.
141 The formation of aragonite is unfavourable at 75 °C, shown by a significant
142 reduction in peak intensity. At this elevated temperature, the formation of a new
143 specie; hydromagnesite ($\text{Mg}_5(\text{CO}_3)_4(\text{OH})_2 \cdot 4\text{H}_2\text{O}$) becomes favourable. The
144 formation of calcium carbonate hydrate (CCH), increases with increased synthesis
145 temperatures, shown by the increasing peak intensity at around $20^\circ 2\theta$. The
146 formation of hydromagnesite and CCH reduces the concentration of available
147 carbonate in solution, and therefore limits the formation of aragonite.

148

149 **Vibrational spectroscopy**

150

151 **Hydroxyl stretching and bending vibrations.**

152

153 The Raman spectra and infrared spectra of the OH stretching region of the Bayer
154 precipitates are shown in Figure 2. Both Raman and infrared band profiles in the
155 hydroxyl stretching region are broad, consisting of multiple overlapping bands.
156 These bands include water in the interlayer between the hydroxyl layers, which
157 may or may not form bridging-type bonds with interlayer anions, water adsorbed
158 on the outer surface, and free water between layers. These broad bands are
159 assigned to the stretching modes of hydroxyl groups in the hydroxyl layers and
160 water molecules associated with the hydrotalcite structure. Band component

161 analysis was used to help identify the different hydroxyl species in both the Raman
162 and infrared spectra.

163

164 The Raman bands in the 3800 to 3000 cm^{-1} region are attributed to the H-bonded
165 stretching vibrations of the OH units of the brucite-like sheets, and stretching
166 vibrations of water molecules. The low intensity bands at 3570 cm^{-1} and the higher
167 intensity bands at 3440 cm^{-1} are assigned to the OH stretching vibrations of OH
168 units in the brucite-like sheets. The Raman bands at 3570, 3565, 3574, and
169 3566 cm^{-1} , for the four precipitates in order of increasing temperature, are assigned
170 to the OH stretching vibrations of $-\text{MgOH}$, while bands at 3445, 3451, 3438, and
171 3438 cm^{-1} are assigned to the OH stretching vibrations of $-\text{AlOH}$ in hydrotalcite
172 and to a small extent hydromagnesite for the 75 °C precipitate.

173

174 The bands in the infrared spectra are at slightly higher wavenumbers and include a
175 couple of additional bands. The infrared spectra of BHT @ 25°C and BHT @
176 55°C are quite similar in appearance, whereas, the spectrum for BHT @ 0°C has
177 one less band, while BHT @ 75°C has two additional sharp small intensity bands.
178 It is proposed that the absence of the additional band for BHT @ 0°C is due to the
179 overlapping of the broad intense peaks, while the additional sharp peaks in BHT
180 @ 75°C is due to two different kinds of OH groups in hydromagnesite. The band
181 at 3519 cm^{-1} is believed to participate in hydrogen bonding, while the other band
182 at 3648 cm^{-1} does not [8]. According to the results obtained by XRD,
183 hydromagnesite only forms at 75 °C. Infrared bands at 3598, 3622, 3643, and
184 3637 cm^{-1} are assigned to the OH stretching vibrations of $-\text{MgOH}$, while bands at
185 3481, 3527, 3561, 3567 cm^{-1} are assigned to the OH stretching vibrations of
186 $-\text{AlOH}$. There is a slight shift to slightly higher wavenumbers, indicating a
187 weakening of the bonding. The other bands within the region 3600 to 3400 cm^{-1} are
188 attributed to the stretching frequencies of hydroxyl groups bonded to Al, Mg or a
189 combination of both.

190

191 The Raman and infrared bands in the region 3400 to 3200 cm^{-1} are assigned to the
192 O-H stretching vibrations of water coordinated to the cations in the brucite-like
193 layers. Bayer precipitates formed at 0 and 25 °C observe an additional Raman
194 band at around 2950 cm^{-1} , assigned to water strongly hydrogen bonded to an anion

195 intercalated into the hydrotalcite interlayer. However, due to the high
196 concentration of carbonate anions in Bayer liquor streams, the band at 2950 cm^{-1} is
197 proposed to be carbonate bonded to water in the hydrotalcite interlayer. Generally
198 these lower wavenumber bands are not observed in Raman spectra, due to water
199 being a very weak Raman scatterer. Raman bands at 3120 , 3097 , 3185 , and
200 3126 cm^{-1} , with increasing temperature, are also attributed to hydrogen bonded
201 water molecules to interlayer anions. The corresponding infrared bands are more
202 intense, due to a large change in dipole moment in water. BHT @ 0°C observed
203 four bands in this lower wavenumber region, 3097 , 2916 , 2769 , and 2596 cm^{-1} .
204 The other Bayer precipitates observed three bands in this lower wavenumber
205 region. Infrared bands at 3097 and 2916 cm^{-1} for BHT @ 0°C , 3034 and
206 2899 cm^{-1} for BHT @ 25°C , 3078 and 2932 cm^{-1} for BHT @ 55°C , and 3172 and
207 2950 cm^{-1} for BHT @ 75°C are believed to be attributed to water hydrogen bonded
208 to interlayer anions in the hydrotalcite interlayer. Infrared bands at around 2700
209 and 2500 cm^{-1} are assigned to the calcium carbonate specie, aragonite and calcium
210 carbonate hydrate. The infrared bands at 2769 and 2703 cm^{-1} , BHT @ 0°C and
211 BHT @ 75°C respectively, are believed to be due to adsorbed water hydrogen
212 bonded with carbonate associated with hydromagnesite, while bands at around
213 2550 cm^{-1} are assigned to water hydrogen bonded to carbonate, associated with
214 aragonite. These assumptions are base on XRD results, which showed the presence
215 of aragonite in all samples, and hydromagnesite in BHT @ 75°C .

216

217 The Raman spectrum of BHT @ 55°C appears to be more compact then the other
218 three samples. It is suggested that a smaller quantity of water is associated with
219 this sample, in particular interlayer water. The d_{003} spacing, found by XRD,
220 showed this Bayer hydrotalcite had the largest interlayer distance, which would
221 indicate a larger quantity of water and anions in the interlayer region. However,
222 the absence of the water band at 2950 cm^{-1} , suggests that the increase in interlayer
223 distance is an increase of intercalated anions rather than water.

224

225 The water deformation modes are observed in the infrared spectra at around
226 1650 cm^{-1} , Figure 3. The Bayer precipitates show water deformations modes at
227 1649 , 1649 , 1651 , and 1657 cm^{-1} , with increasing temperature, attributed to
228 interlayer water hydrogen bonded to interlayer anions. The position of this band

229 appears to shift to slightly higher wavenumbers for the precipitates formed at 55
230 and 75 °C, indicating a strengthening of the hydrogen bond. The position of these
231 bands suggests that interlayer water is hydrogen bonded to carbonate and possibly
232 sulfate [9].

233

234 **Carbonate vibrational region.**

235

236 The Raman spectra in the 1200 to 900 cm^{-1} region show multiple bands at around
237 1085 cm^{-1} attributed to the (CO_3^{2-}) symmetric stretching vibrations, Figure 4. Four
238 normal modes of free carbonate exist: the ν_1 symmetric stretch of A_1 symmetry
239 normally observed at 1063 cm^{-1} , the antisymmetric stretch of E' observed at
240 1415 cm^{-1} , the ν_2 out of plane bend at 680 cm^{-1} [8]. All modes are Raman and
241 infrared active except for the ν_2 mode, which is infrared active only. The
242 intercalation of carbonate anions into the hydrotalcite structure causes a shift
243 towards lower wavenumbers, due to the interaction of carbonate with interlayer
244 water molecules and/or hydroxyl groups from the brucite-like layer.

245

246 The Raman band profiles for the carbonate symmetric stretching vibrations clearly
247 show the formation of calcite and aragonite at varying temperatures. The most
248 simplistic profile is observed for BHT @ 25°C, with a sharp intense band at 1085
249 cm^{-1} , and a broad shoulder at around 1060 cm^{-1} . The sharp band at 1085 cm^{-1} ,
250 observed in all precipitates, is assigned to the symmetric stretching mode of
251 carbonate in aragonite. The bands at around 1060 cm^{-1} are assigned to hydrotalcite
252 and are due to the symmetric stretching mode of carbonate anions bonded to
253 interlayer water. Raman bands at around 1090 and 1100 cm^{-1} for the three other
254 precipitates are assigned to CCH. These values are in good agreement with
255 literature [8]. The shift towards higher wavenumbers indicates stronger hydrogen
256 bonding of the carbonate ion occurs at increased temperatures.

257

258 The overall band profile in the infrared spectra for the carbonate antisymmetric
259 vibrational region, Figure 3, consists of two or three overlapping bands.

260 Determination of these bands proved to be more difficult than those in the Raman
261 spectra, however the following assignments have been made based on literature

262 and XRD results found in this study. Bands at around 1400 and 1360 cm^{-1} are
263 assigned to carbonate incorporated into the hydrotalcite interlayer. BHT @ 75°C
264 has a significantly different shape, due to the sharp peaks at around 1480 and
265 1420 cm^{-1} . These sharp bands are assigned to the carbonate antisymmetric
266 stretching mode of hydromagnesite. Infrared bands around 1420 cm^{-1} are assigned
267 to calcite [10]. The broader bands at 1477, 1477, 1486, and 1484 cm^{-1} , with
268 increasing temperature, are assigned to aragonite, reported in literature to be
269 situated at 1493-70 and 1450-30 cm^{-1} [10]. The shoulder at around 1520 cm^{-1} is
270 also assigned to aragonite and possibly a minor contribution from carbonate in
271 hydrotalcite. XRD results showed only a minor quantity of aragonite present in
272 BHT @ 75°C, and the absence of the peak at 1520 cm^{-1} for this precipitate,
273 indicates that this peak is predominantly due to the antisymmetric stretch of
274 carbonate in aragonite and not hydrotalcite.

275

276 There appear to be two peaks in the 1000 to 900 cm^{-1} region for all four
277 precipitates, proposed to be sulfate anions intercalated into the hydrotalcite
278 structure. A tetrahedral ion, such as sulfate, has four modes of vibration when it
279 retains its full (T_d) symmetry; these are the symmetric stretching (ν_1) modes
280 observed at 983 cm^{-1} , the ν_2 bending mode observed at 450 cm^{-1} , the ν_3 mode at
281 1105 cm^{-1} , and the ν_4 mode at 611 cm^{-1} . The ν_1 and ν_2 modes are Raman active
282 only, whereas the ν_3 and ν_4 modes are both infrared and Raman active. The Raman
283 bands at 990 and 980 cm^{-1} are assigned to the ν_1 S-OH stretch of the sulfate anions
284 in the hydrotalcite interlayer. The two different peaks suggest that sulfate anions
285 exist in two different environments within the hydrotalcite interlayer. The band at
286 990 cm^{-1} is proposed to be sulfate anions bonding with the cationic surface of the
287 brucite-like sheets, while the band at 980 cm^{-1} is assigned to sulfate anions hydrogen
288 bonded to interlayer water. The intercalation of other anionic specie is not
289 identified in this study. There are a limited number of intercalation sites in the
290 hydrotalcite interlayer, and the intense competition of the high affinity anions
291 sulfate and carbonate limits the intercalation of other anions.

292

293

294

295 **Cation OH deformation modes.**

296

297 An intense Raman band at 550 cm^{-1} with a shoulder at 565 cm^{-1} , figure not shown,
298 are assigned to the $\text{Al}(\text{OH})_6$ unit in hydrotalcite due to the vibration of aluminium-
299 oxygen bonds. No apparent changes are detectable in these bands, and therefore, it
300 is proposed that the synthesis temperature has a minimal effect on the brucite-like
301 sheets of the hydrotalcite structure. Raman bands at around 470 cm^{-1} are assigned
302 to the Mg-O-Mg linkage bonds in hydrotalcite.

303

304 **CONCLUSIONS**

305

306 The seawater neutralisation of supernatant liquor resulted in the formation of a
307 variety of mineralogical phases, including hydrotalcite-like structures,
308 hydromagnesite, and two forms of calcium carbonate. XRD showed that the
309 crystallinity of the Bayer hydrotalcite decreased with increasing temperature,
310 shown by the broadening of the $60^\circ 2\theta$ peak and the reduction in peak intensities.
311 Bayer hydrotalcites formed at 55°C observed the largest basal spacing, indicating
312 a larger concentration of anions and water are intercalated into BHT @ 55°C .
313 Therefore, the precipitation of Bayer hydrotalcites at 55°C appears to be the most
314 effective at removing dissolved anions from Bayer liquors via intercalation.
315 Results show that Bayer hydrotalcites are formed at all temperatures investigated,
316 with minor amounts of manasseite forming at higher temperatures. Raman
317 spectroscopy showed a reduction in the amount of aragonite that forms 75°C ,
318 whilst the formation of hydromagnesite and calcite increased.

319

320 The presence of bands at 3000 cm^{-1} in the Raman spectra, indicate Bayer
321 hydrotalcites have large quantities of interlayer water. However, the absence of
322 this peak in BHT @ 55°C and a large basal spacing, suggests that the interlayer
323 region is composed of a smaller percentage of interlayer water and a higher
324 percentage of interlayer anions. This characteristic is responsible for the removal
325 of anions in Bayer liquor streams.

326

327 The position of the water deformation modes indicate that interlayer water is
328 hydrogen bonded to carbonate and sulfate. The intercalation of sulfate anions is
329 confirmed by the presence of Raman bands at around 990 and 980 cm^{-1} . The
330 intercalation of other anionic species is not identified by the techniques used in
331 this study.

332

333

334 **ACKNOWLEDGEMENTS**

335

336 The financial and infra-structure support of the Queensland Research and
337 Development Centre (QRDC-RioTintoAlcan) and the Queensland University of
338 Technology Inorganic Materials Research Program of the School of Physical and
339 Chemical Sciences are gratefully acknowledged.

340

341 **REFERENCES**

342

- 343 1. C. Hanahan, D. McConchie, J. Pohl, R. Creelman, M. Clark and C. Stocksiek,
344 Environ. Eng. Sci., **21**, 125-138, (2004).
- 345 2. U. Costantino, F. Marmottini, M. Nocchetti and R. Vivani, Eur. J. Inorg.
346 Chem., **10**, 1439-1446, (1998).
- 347 3. R. L. Frost, Z. Ding and J. T. Kloprogge, Can. J. Anal. Sci. Spectros., **45**, 96-
348 102, (2000).
- 349 4. R. L. Frost and K. L. Erickson, J. Therm. Anal. Calorim., **76**, 217-225, (2004).
- 350 5. S. J. Palmer and R. L. Frost, J. Mater. Sci., **44**, 55-63, (2009).
- 351 6. J. Palmer Sara, A. Soisonard and L. Frost Ray, J. Colloid Interface Sci., **329**,
352 404-409, (2009).
- 353 7. S. J. Palmer, R. L. Frost, G. Ayoko and T. Nguyen, J. Raman Spectrosc., **39**,
354 395-401, (2008).
- 355 8. V. C. Farmer, "Mineralogical Society Monograph 4: The Infrared Spectra of
356 Minerals", Mineralogical Society, London, (1974).
- 357 9. V. Rives, "Layered Double Hydroxides: Present and Future", Nova Science,
358 New York, (2001).
- 359 10. J. A. Gadsden, "Infrared Spectra of Minerals and Related Inorganic
360 Compounds", Butterworth, London, (1975).

361

362

363

364

365

366

367

368

369

370

371

372

373

374

375 **LIST OF TABLES**

376

377 Table 1: Chemical composition of SNL and seawater.

378

379 **LIST OF FIGURES**

380

381 Figure 1: XRD patterns of Bayer precipitates synthesised at different temperatures via
382 the SWN process.

383 Figure 2: Raman and infrared spectra of Bayer precipitates in the hydroxyl stretching
384 region.

385 Figure 3: Raman spectra of Bayer precipitates in the 1200-900 cm^{-1} region.

386 Figure 4: Infrared spectra of Bayer precipitates in the 1800-1200 cm^{-1} region.

387

388

389

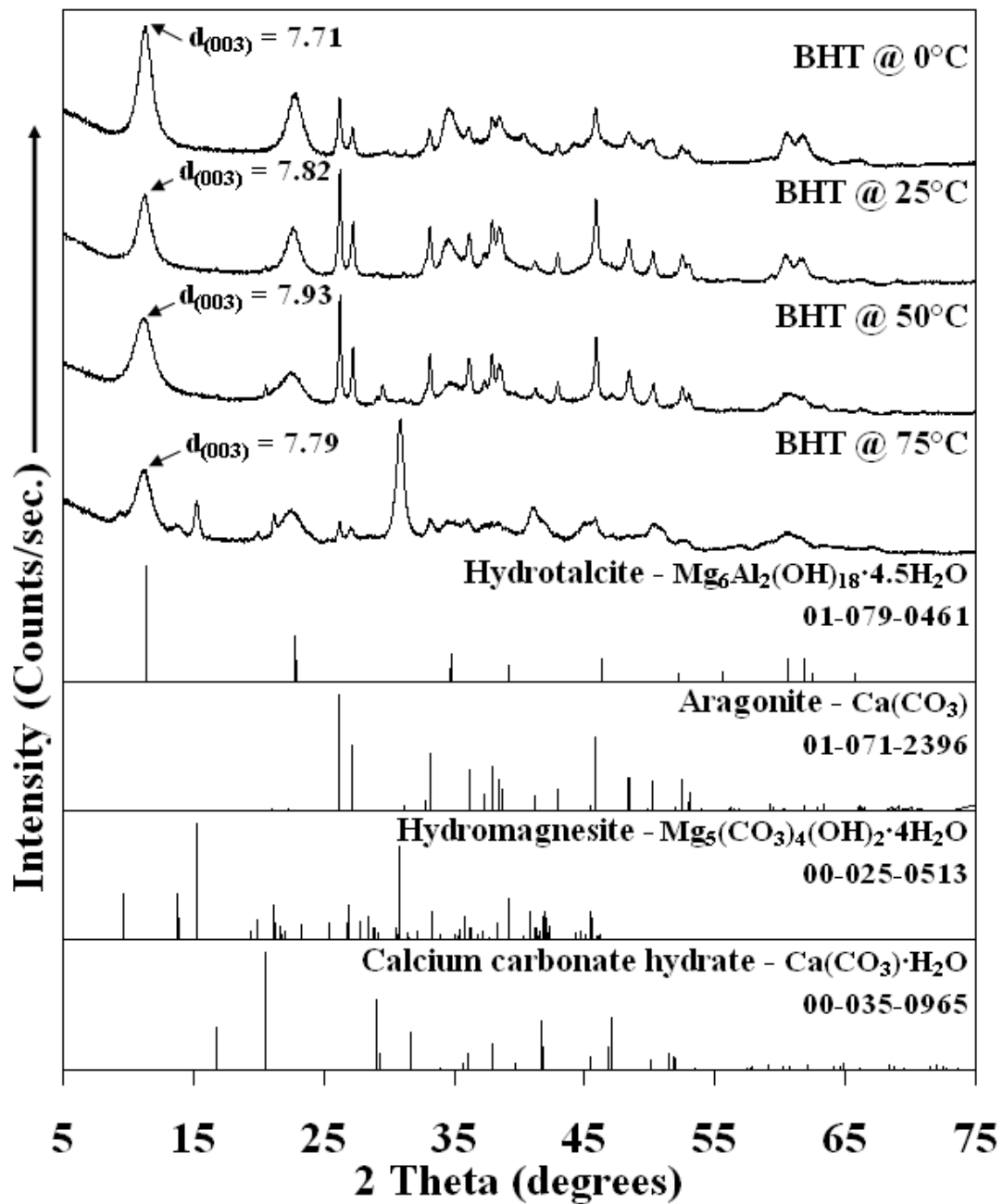
390 **TABLES**

391

392 Table 1: Chemical composition of SNL and seawater.

Cation/Anion	Concentration
SNL	
Al³⁺	2.8 (g/L Al₂O₃)
OH⁻	3.0 (g/L Na₂O)
CO₃²⁻	9.9 (g/L Na₂O)
Seawater	
Mg²⁺	1295 ppm
Ca²⁺	416 ppm
SO₄²⁻	2701 ppm
HCO₃⁻	145 ppm
Cl⁻	19345 ppm

393

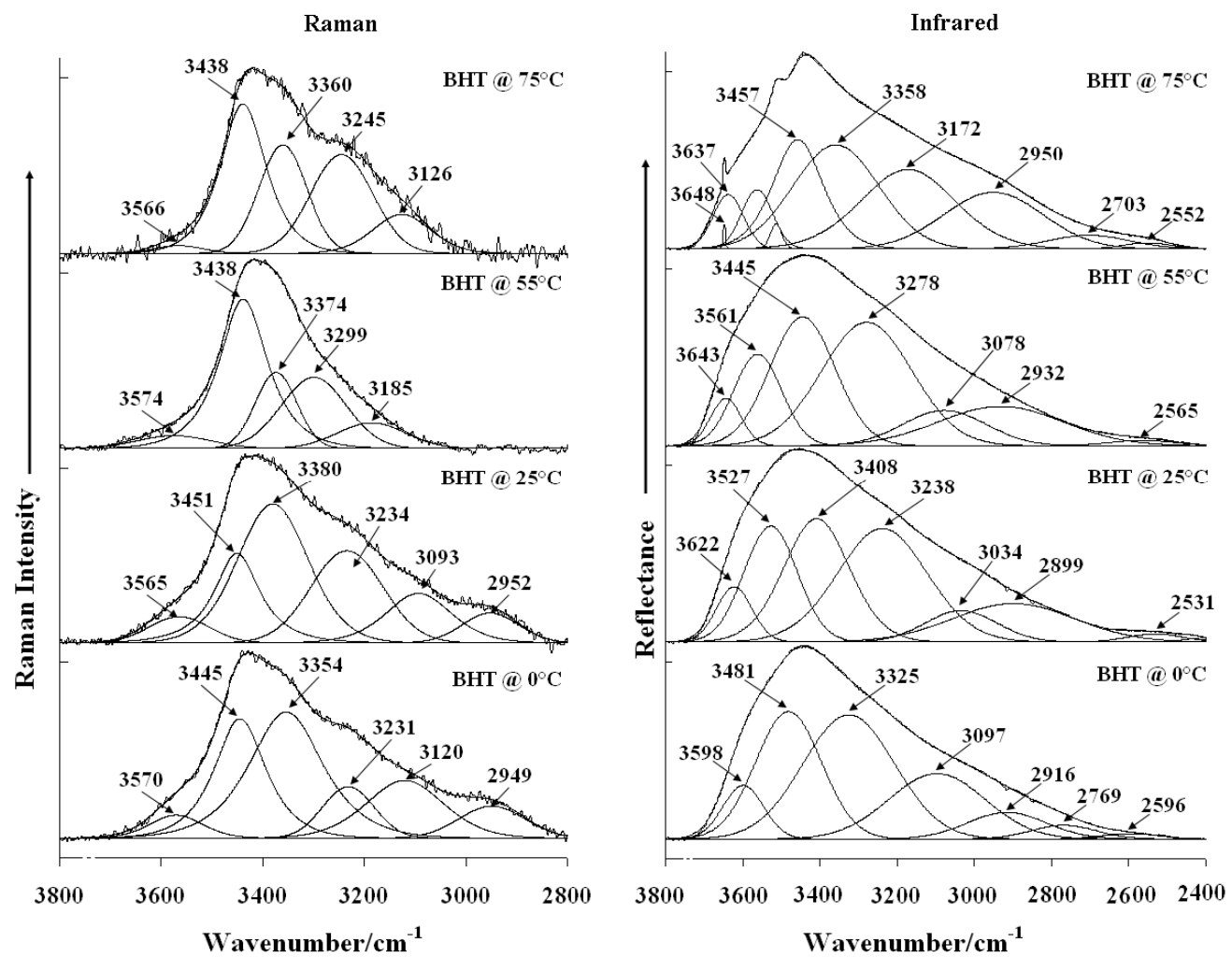


395

396 Figure 1: XRD patterns of Bayer precipitates synthesised at different temperatures

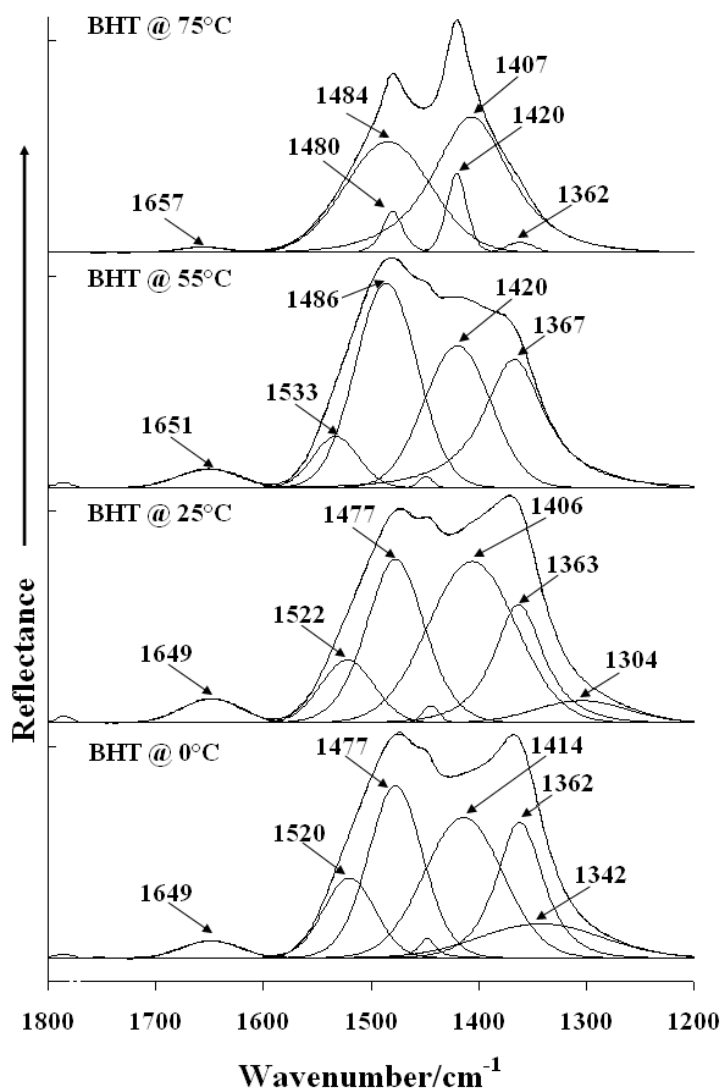
397

via the SWN process.



398

399 Figure 1: Raman and infrared spectra of Bayer precipitates in the hydroxyl stretching region.

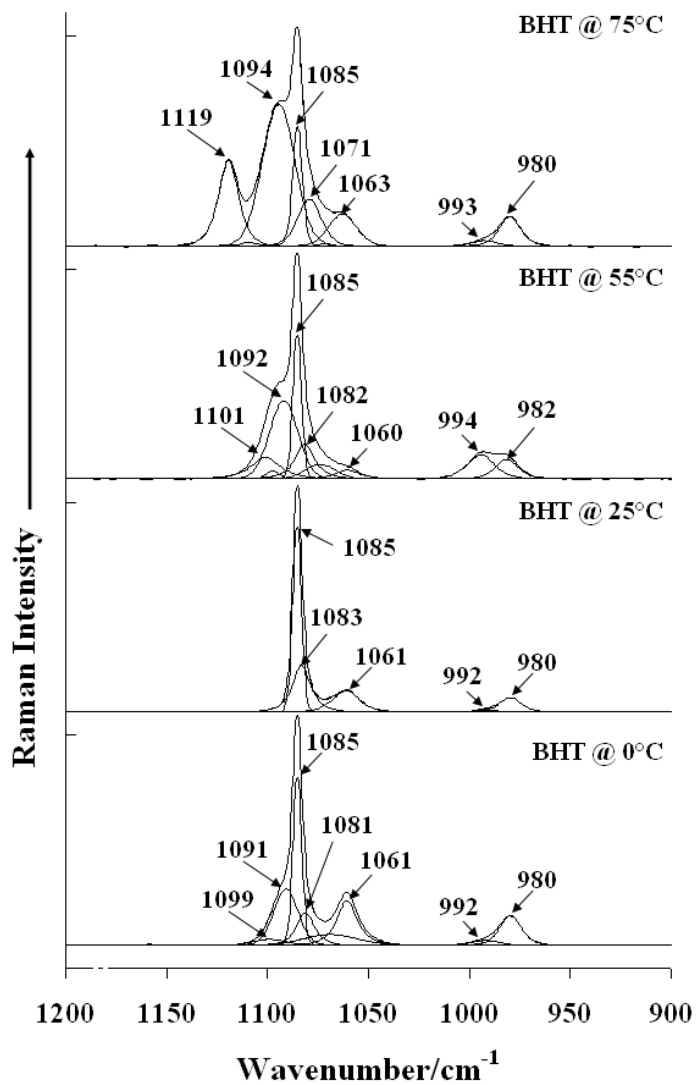


400

401 Figure 3: Infrared spectra of Bayer precipitates in the 1800 - 1200 cm⁻¹ region.

402

403



404

405 Figure 4: Raman spectra of Bayer precipitates in the 1200 - 900 cm⁻¹ region.